Joule

CellPress

Article

Air-Breathing Aqueous Sulfur Flow Battery for Ultralow-Cost Long-Duration Electrical Storage

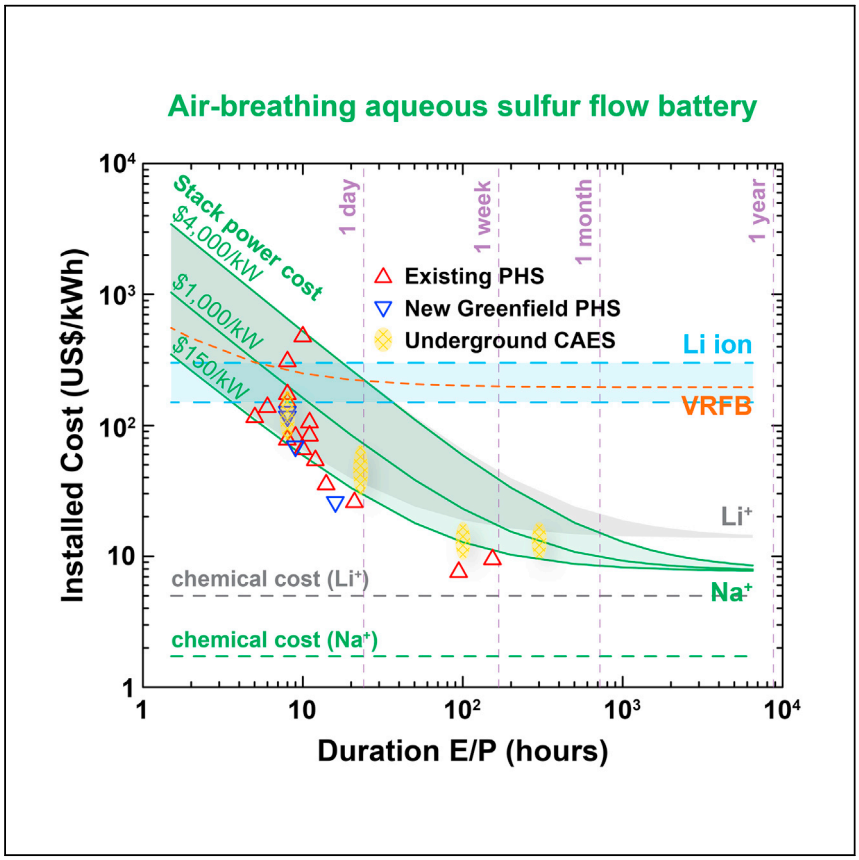

The dropping cost of wind and solar power intensifies the need for low-cost, efficient energy storage, which together with renewables can displace fossil fuels. While batteries for transportation and portable devices emphasize energy density as a primary consideration, here, low-cost, ultra-abundant reactants deployable at massive (TWh) scale are essential. An air-breathing aqueous sulfur flow battery approach with ultralow energy cost is demonstrated at laboratory scale and shown to have economics similar to pumped hydroelectric storage without its geographical and environmental limitations.

Zheng Li, Menghsuan Sam Pan, Liang Su, ..., Kai Xiang, Fikile R. Brushett, Yet-Ming Chiang

ychiang@mit.edu

HIGHLIGHTS

Chemical cost analyzed for 40 rechargeable couples developed over the past 60 years

Aqueous sulfur/sodium/air system identified with ultralow chemical cost of ~US$1/kWh

Air-breathing flow battery architecture demonstrated at laboratory scale

Techno-economic analysis shows installed cost is comparable with PHS and CAES

Li et al., Joule 1, 306–327
October 11, 2017
https://doi.org/10.1016/j.joule.2017.08.007

Joule

CellPress

Article

Air-Breathing Aqueous Sulfur Flow Battery for Ultralow-Cost Long-Duration Electrical Storage

Zheng Li,[1,3] Menghsuan Sam Pan,[1,3] Liang Su,[2,3] Ping-Chun Tsai,[1] Andres F. Badel,[2] Joseph M. Valle,[1] Stephanie L. Eiler,[1] Kai Xiang,[1] Fikile R. Brushett,[2] and Yet-Ming Chiang[1,4,*]

SUMMARY

The intermittency of renewable electricity generation has created a pressing global need for low-cost, highly scalable energy storage. Although pumped hydroelectric storage (PHS) and underground compressed air energy storage (CAES) have the lowest costs today (~US$100/kWh installed cost), each faces geographical and environmental constraints that may limit further deployment. Here, we demonstrate an ambient-temperature aqueous rechargeable flow battery that uses low-cost polysulfide anolytes in conjunction with lithium or sodium counter-ions, and an air- or oxygen-breathing cathode. The solution energy density, at 30–145 Wh/L depending on concentration and sulfur speciation range, exceeds current solution-based flow batteries, and the cost of active materials per stored energy is exceptionally low, ~US$1/kWh when using sodium polysulfide. The projected storage economics parallel those for PHS and CAES but can be realized at higher energy density and with minimal locational constraints.

INTRODUCTION

The rapidly dropping cost of wind and solar electricity generation, as illustrated by levelized costs of electricity (LCOE) that are now competitive, or nearly so, with fossil fuel generation,[1] highlights the need for low-cost electrical storage that can transform intermittent renewable power into predictable and dispatchable electricity generation, and potentially even baseload power. Such a revolutionary outcome will require energy storage with costs well below the trajectory of current technology, while also being safe, scalable, long-lived, and sufficiently energy dense for widespread deployment, including in space-constrained environments. Emerging use-case studies suggest that installed costs of <$50/kWh, operating over multi-day or longer durations, will be required for renewable-based generation to compete economically with existing fossil plants on a drop-in basis. It is unclear whether electrochemical storage can meet these challenges.

Here, we first review the underlying chemical cost of energy storage for about 40 electrochemical couples representing all major classes of rechargeable batteries developed over the past 60 years. From this analysis, it is clear that the best opportunities for overcoming the above challenges reside with electrochemical couples that use ultralow-cost, highly abundant raw materials. Among these, sulfur has the 14th highest crustal abundance and is widely available as a byproduct of natural gas and petroleum refining.[2] Sulfur also has the lowest cost per stored charge of known redox active materials, next to water and air (see Table S1; in US$/kAh, sulfur

Context & Scale

Wind and solar generation can displace carbon-intensive electricity if their intermittent output is cost-effectively reshaped using electrical storage to meet user demand. Reductions in the cost of storage have lagged those for generation, with pumped hydroelectric storage (PHS) remaining today the lowest-cost and only form of electrical storage deployed at multi-gigawatt hour scale. Here, we propose and demonstrate an inherently scalable storage approach that uses sulfur, a virtually unlimited byproduct of fossil fuel production, and air, as the reactive components. Combined with sodium as an intermediary working species, the chemical cost of storage is the lowest of known batteries. While the electrical stacks extracting power can and should be improved, even at current performance, techno-economic analysis shows projected costs that are competitive with PHS, and of special interest for the long-duration storage that will be increasingly important as renewables penetration grows.

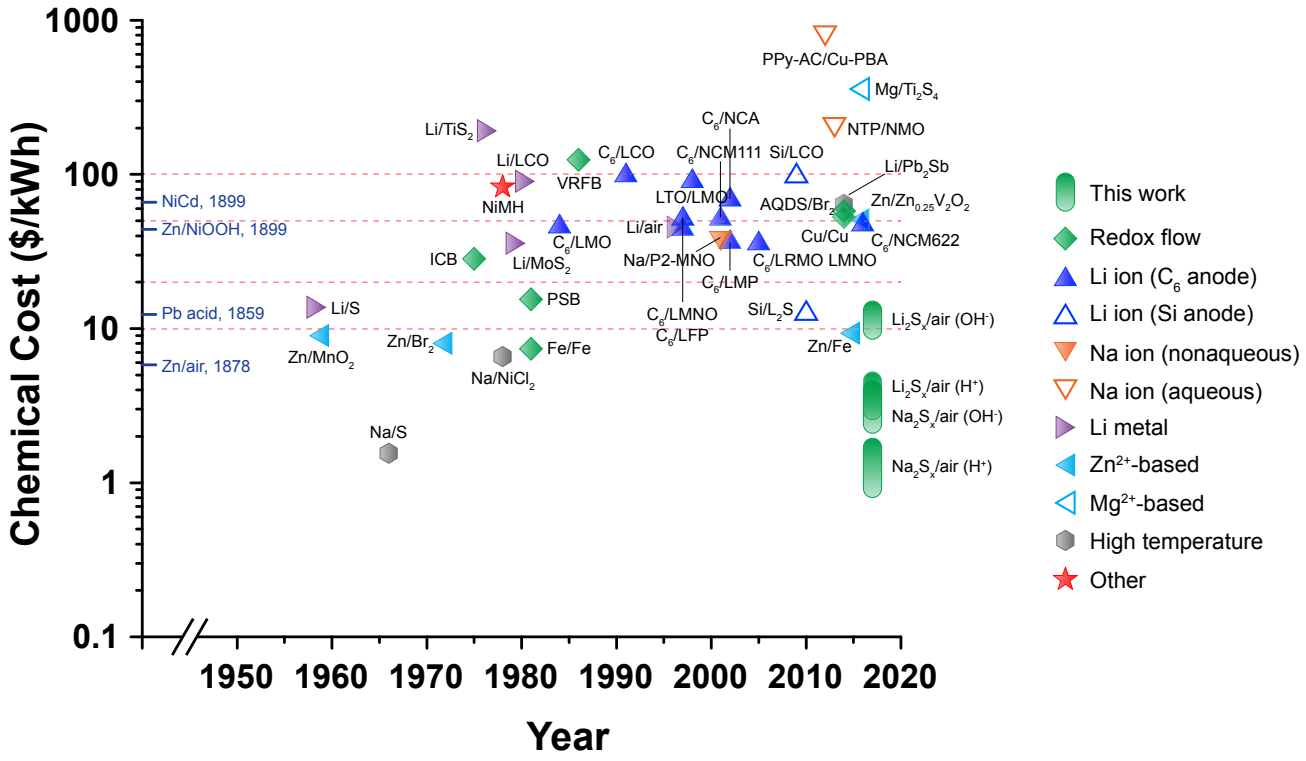

Figure 1. The Chemical Cost of Storage (US$/kWh) for Representative Classes of Rechargeable Batteries, Shown against the Year of Introduction

Chemical cost represents a floor on the cost of the complete battery and is computed here from the unit costs (e.g., US$/kg) of the cathode-active material, anode-active material, and electrolyte, normalized to the stored energy (e.g., Wh/kg). Exemplars of each of the major rechargeable battery families are included. Numerical values and electrochemical details are given in Table S2, and details of the calculations appear in Supplemental Information. For the present approach, Li_2S_x/air and Na_2S_x/air, the range of costs shown represents varying utilization of the theoretical sulfur capacity from 25% to 50%.

0.15, zinc 3.66, graphite 32.27, and $LiCoO_2$ 292.14). In this work, we demonstrate an ambient-temperature, air-breathing, aqueous polysulfide flow battery that exploits sulfur's intrinsic advantages, and show using techno-economic analyses that such an approach has the potential to meet future storage needs for renewable energy.

RESULTS AND DISCUSSION

Chemical Cost Comparison for Battery Electrochemistries

A reasonable starting point for bottom-up analysis of the economics of any battery technology is the cost of the cathode, anode, and electrolyte, normalized to the stored electrical energy. We define this quantity as the chemical cost of energy storage (abbreviated as chemical cost and given in US$/kWh), building on an earlier study[3] that analyzed the elemental costs of electrochemical couples. The chemical cost for about 40 battery chemistries is plotted in Figure 1 against the year that each electrochemistry was introduced (all costs are in 2017 US$). Although we have not attempted to exhaustively list all extant electrochemical couples, exemplars of each of the major classes of bulk rechargeable batteries are included. The numerical results plotted in Figure 1 are tabulated in Table S2, and details of the calculations, including input parameters, key assumptions, and literature sources, are given in the Supplemental Information.

A striking result apparent in Figure 1 is that the chemical cost of new battery chemistries has in general systematically increased rather than decreased over 60 years

[1]Department of Materials Science and Engineering, Massachusetts Institute of Technology, Cambridge, MA 02139, USA

[2]Department of Chemical Engineering, Massachusetts Institute of Technology, Cambridge, MA 02139, USA

[3]These authors contributed equally

[4]Lead Contact

*Correspondence: ychiang@mit.edu

https://doi.org/10.1016/j.joule.2017.08.007

of battery development. We believe that to a large extent this trend can be attributed to the pursuit of higher energy density, as exemplified by the deployment of Li-ion batteries in portable device and transportation applications once dominated by NiMH, NiCd, or Pb-acid batteries. Figure 1 shows that Li-ion technology itself spans nearly a 3-fold range of chemical cost, from ~US$35/kWh ($C_6$/$0.3Li_2MnO_3$-$0.7LiMn_{0.5}Ni_{0.5}O_2$) to ~ US$100/kWh (C_6/$LiCoO_2$). Given that energy density has generally increased over time, the rising chemical cost implies that the high cost of new materials has more than compensated. Figure 1 also shows that while several aqueous electrochemical couples have chemical cost below US$10/kWh, the lowest cost of which is Zn-air, which as a primary chemistry dates to the year 1878, several aqueous electrochemical couples have chemical costs greater than low-cost Li-ion. This again reflects the high cost of synthesized active materials relative to stored energy. The case of Na/S is instructive; while it has the lowest chemical cost in our plot, excluding present results, it is known that high-temperature Na/S batteries are among the most expensive at system level (~US$800/kWh). This is due to the high cost of supporting components and balance of plant. Conversely, an ambient-temperature sodium-sulfur chemistry has the potential for exceptionally low system cost, given a starting chemical cost of ~US$1/kWh. These considerations led us to explore new ambient-temperature alkaline-sulfur chemistries, culminating in the air-breathing aqueous polysulfide couples, denoted in Figure 1 as Li_2S_x/air and Na_2S_x/air, the lowest-cost members of which have <US$1/kWh chemical cost.

Air-Breathing Aqueous Polysulfide Concept

Whereas nonaqueous lithium-sulfur[4–6] and high-temperature sodium-sulfur batteries[7] use sulfur as the cathode, an all-aqueous system must use sulfur as the anode material to preserve aqueous stability while reaching a meaningful cell voltage. Solubilized aqueous sulfur electrodes have previously been paired with halogenated catholytes in flow batteries,[8–10] used as the catholyte versus "protected" lithium metal anodes,[11] and used as the anolyte with lithium intercalation cathodes.[12,13] (Here, "anode" and "cathode" refer to solid-phase active materials, whereas "anolyte" and "catholyte" refer to fluids with solubilized active materials.) In each of these cases, the chemical cost of storage is dominated by the nonsulfur electrode. Thus, we reasoned that if aqueous anolytes of highly soluble metal polysulfides (up to 12 M)[11] could be matched with a similarly low-cost catholyte, unprecedented low storage economics could be achieved. Our scheme, illustrated in Figure 2, is an aqueous flow battery that pairs a polysulfide anolyte with an oxygenated/aerated salt solution as the catholyte. At the anolyte side, charge transfer occurs to a negative current collector connected to the external circuit. At the catholyte side, a single or dual oxygen evolution/reduction cathode configuration is used. This configuration pairs two half-reactions, namely polysulfide oxidation/reduction and oxygen evolution reaction (OER)/oxygen reduction reaction (ORR), which unlike conventional rechargeable couples, do not share a common working ion.

Specifically, during operation, Li^+ and Na^+ (or other metal ions) shuttle between the electrolytes. In the anolyte, these working ions participate in the polysulfide redox reactions. In the catholyte, in order to maintain electroneutrality, ions are generated or consumed through oxygen electrochemistry, using water as both solvent and reactant. The reversible capacity of the cell is determined by either the total concentration of alkali-metal ions, or by the sulfur concentration in the anolyte, whichever is limiting. The generation and consumption of protons (for acid catholyte) or hydroxyls (for alkaline catholyte) lead to pH swings in the catholyte.

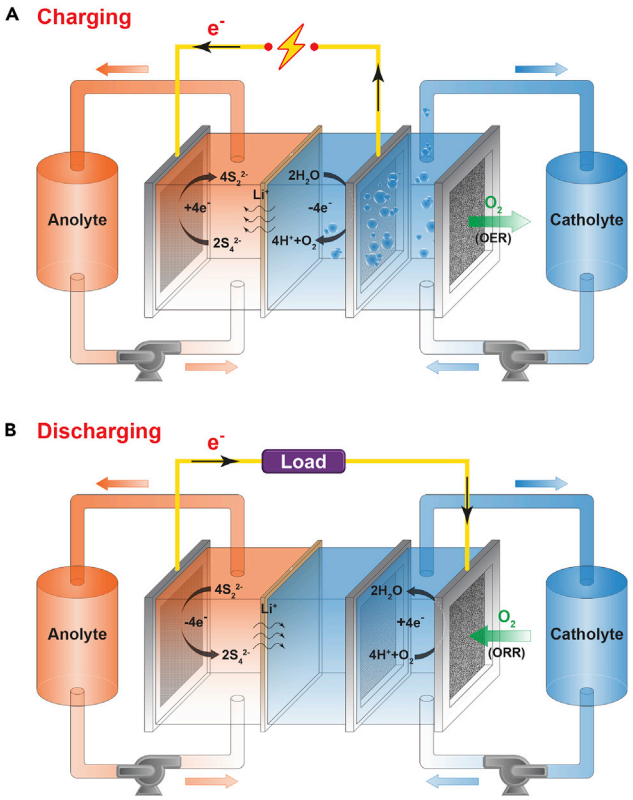

Figure 2. Air-Breathing Aqueous Sulfur Flow Battery Concept

The anolyte (left) is an aqueous polysulfide solution within which the working ions (here, Li^+ or Na^+) carry out the sulfur redox reaction. The catholyte (right) is an acidic or alkaline solution containing the working ion as a dissolved salt, e.g., Li_2SO_4 or Na_2SO_4.

(A) Upon charging, oxygen evolution occurs as the H^+ concentration increases to accommodate the loss of working ions.

(B) Upon discharging, oxygen reduction occurs, and the catholyte is enriched in working ions.

In the alkaline catholyte case, hydroxyl crossover is not anticipated to be detrimental to performance, while in the acid catholyte case, protons must be confined to the catholyte chamber to prevent mixing with the alkaline anolyte. Here, we use ceramic membranes as the separators. Note that this scheme is not a sulfur-air battery, as there is no direct reaction between any sulfur species and oxygen. We searched for related concepts in the literature, and found a recently proposed Zn-air battery that also utilizes acidic catholyte and alkaline anolyte separated by a solid electrolyte (LiSICON) membrane,[14] but in a stationary (non-flowing) design. We also found a published patent application[15] that proposes an all-alkaline flow cell in which an air cathode is paired with a solid sulfur-polysulfide anode; here the working ions are hydroxyl ions and the system requires an anion exchange membrane.

In the present approach, cells may be assembled in the discharged state, in which case the alkali-metal working ion is provided by one of several possible low-cost salts dissolved in the catholyte. In the examples below we use Li_2SO_4 and Na_2SO_4. Cells may also be assembled in the charged state, in which case the working ion is provided by lithium or sodium sulfide dissolved in the anolyte. To avoid H_2S formation at the anolyte, adequately high pH (≥ 12) is maintained by the addition of a suitable base (here, LiOH or NaOH). The catholyte may be either acidic or alkaline, providing

cell voltages of ~1.68 V and ~0.85 V, respectively, at standard state equilibrium, as explained via the cell reactions.

Acidic Catholyte

$$\text{Cathode:}\quad 2H_2O \rightleftarrows O_2\uparrow + 4H^+ + 4e^-, \quad E_c^0 = 1.229 \text{ V versus SHE}$$
$$\text{Anode:}\quad xS_y^{2-} + 2(y-x)e^- \rightleftarrows yS_x^{2-}, \quad E_A^0 = -0.447 \text{ V versus SHE}$$

Alkaline Catholyte

$$\text{Cathode:}\quad 4OH^- \rightleftarrows O_2\uparrow + 2H_2O + 4e^-, \quad E_c^0 = 0.401 \text{ V versus SHE}$$
$$\text{Anode:}\quad xS_y^{2-} + 2(y-x)e^- \rightleftarrows yS_x^{2-}, \quad E_A^0 = -0.447 \text{ V versus SHE}$$

In between these limits, the equilibrium cell voltage varies continuously with pH as shown in the Pourbaix diagram in Figure S1; i.e., it is ~1.26 V at neutral pH.

In order to determine the chemical cost, the stable speciation range of the polysulfide must be taken into account. Although polysulfide solubilities in aqueous solutions can reach as high as 12 M sulfur concentration,[11] stability issues (see below) may limit the practical capacity to less than that for complete reduction of sulfur according to the reaction 2A + S → A_2S (where A is Li or Na). However, even with a more limited range of sulfur reduction, exceptionally low chemical cost is attainable while reaching energy densities higher than many previous flow batteries. This is shown in Tables S4 and S5, where energy density and chemical cost for catholytes and anolytes having 5 M of Li or Na and 5 M of S, respectively, have been calculated. If the entire sulfur reduction capacity is utilized, the energy densities are 121 and 58 Wh/L for acidic and alkaline catholyte, respectively. Increasing the anolyte S concentration to 10 M raises the upper bound to about 145 Wh/L and 70 Wh/L for acidic and alkaline catholyte, respectively. If cycling is restricted to just 25% of the full sulfur reduction capacity, the corresponding energy densities are 60 and 29 Wh/L when using acidic and alkaline catholyte, respectively. This capacity range corresponds to the solution range Li_2S_2-Li_2S_4 or Na_2S_2-Na_2S_4, for which we later demonstrate stable cycling over ~1,000 hr. For sodium-polysulfide chemistry, the chemical cost is remarkably low, only US$0.4–1.7/kWh (using acidic catholyte at 5 M S), depending on the utilization of sulfur theoretical capacity (100%–25%). At 50% utilization or higher, one reaches the lowest chemical cost to our knowledge of any rechargeable battery (Figure 1). When using lithium polysulfide rather than sodium polysulfide, the chemical cost is US$2.0–5.0/kWh, still lower than existing flow batteries.

In the remainder of the paper, we first demonstrate key performance characteristics of the proposed electrochemical couples. Since both catholyte and anolyte are fluids, our electrochemical couples lend themselves to a flow battery design, which is also demonstrated. An attribute of flow batteries is the ability to independently size the power stack and chemical storage capacity to meet desired energy to power ratios. In such architecture, the contribution to system cost of the power stack can be minimized by sizing it only as large as is necessary to meet the maximum power requirement. Using the methodology in a recent techno-economic analysis of flow batteries,[16,17] we show that the proposed electrochemical storage system has attractive performance and cost attributes very similar to those of pumped hydroelectric storage (PHS) and underground compressed air energy storage (CAES), which are currently the lowest-cost energy storage technologies.[18] Finally, the exceptionally low chemical cost allows electrochemical storage to address a new

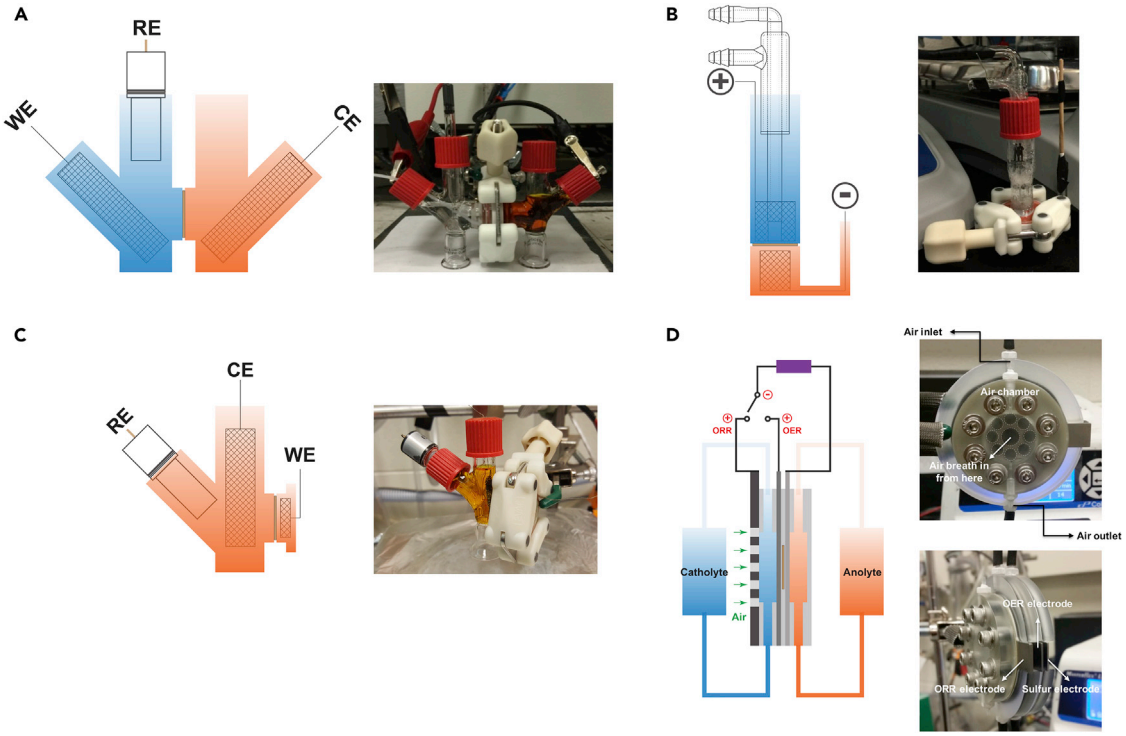

Figure 3. Test Cell Configurations Used in This Work

(A) Standard H cell. Catholyte is in the left chamber and polysulfide in the right chamber in the photograph. The cell membrane area is ~1.5 cm^2 and the electrolyte volume is ~5 mL.

(B) Modified H cell for catholyte long-term cycling. The cell membrane area is ~1.5 cm^2 and the catholyte volume is reduced to ~0.5 mL to permit deep cycling at reasonable current densities.

(C) Modified H cell for anolyte long-term cycling with different chamber volumes; the smaller chamber is deeply cycled.

(D) Flow cell with simultaneous gas exchange and liquid flow of catholyte and anolyte.

domain of long-duration discharge that was not previously accessible in a cost-effective manner.

Verifying the Catholyte and Anolyte Reactions

Using H cells (Figure 3A), we confirmed that OER/ORR occurs at the catholyte side by observing the changes in cell voltage induced by changing the gas composition or by cycling the gas flow on and off. An immediate response of the cell voltage to a change in gas flow conditions is clearly seen in Figures 4A and 4B for acidic and alkaline catholyte, respectively. Then, to determine whether the charge-storing capacity of the catholyte corresponds to the concentration of added salt (Li_2SO_4 or Na_2SO_4), cells with an excess of anolyte were prepared using the modified H-cell design in Figure 3B. Results in Figures 4C and 4D show that the measured capacity of these cells corresponds almost exactly to the theoretical capacity calculated from the Li^+ or Na^+ concentration. In addition, the cell voltage is the same for both alkali ions, as expected from the cell reactions. In the anolyte, polysulfide redox activity was readily discerned from changes in color with state of charge.

Cell Efficiency, Impedance, and Power Density

The voltage efficiency of the cells is determined by the OER/ORR reaction as well as other contributions to cell impedance. To separate these, we first measured the voltage efficiency as a function of current density and temperature, using the standard H cells as well as a cell with separate reference electrodes for the cathode

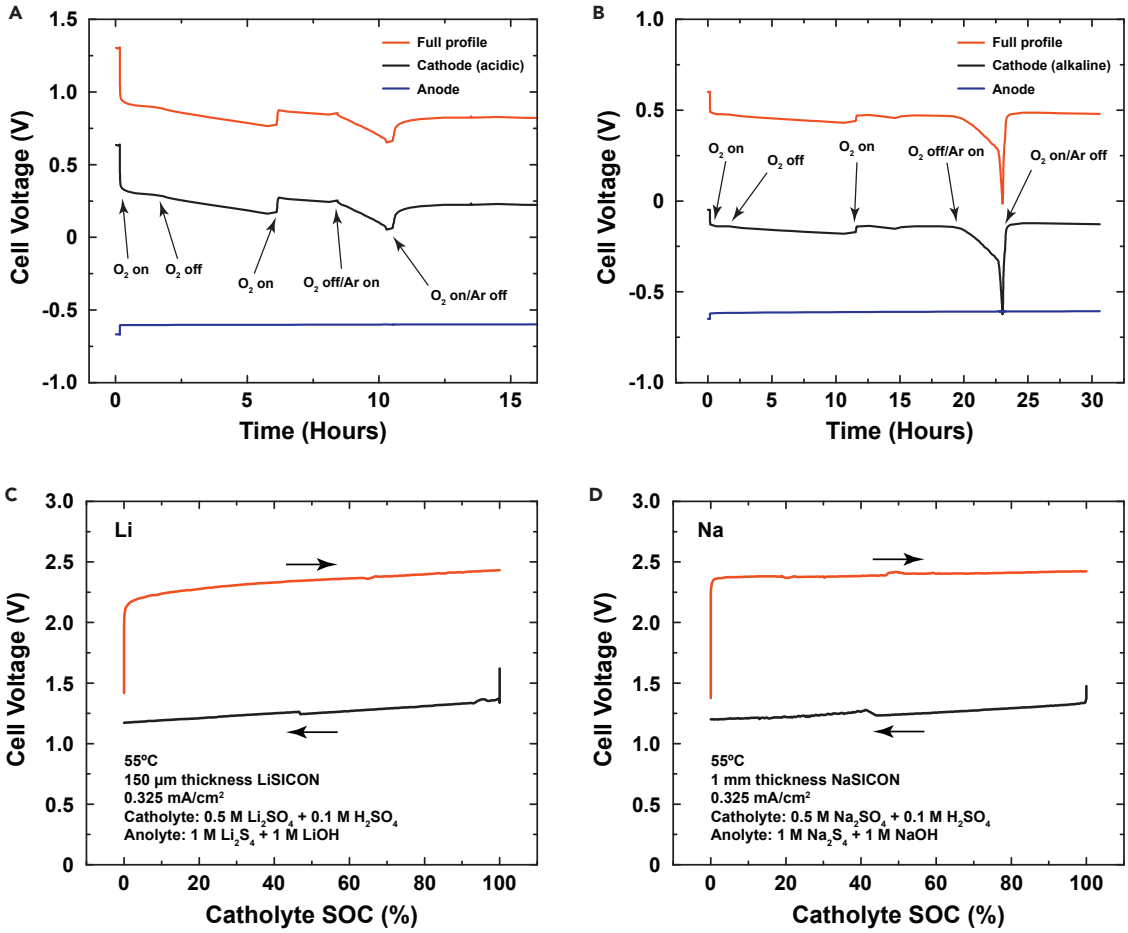

Figure 4. Demonstration of ORR as the Catholyte Discharge Reaction and Catholyte Capacity Limited Full Cells Based on Li- and Na-Salt Chemistries

(A–D) Confirmation of ORR as the catholyte discharge reaction for cells with (A) acidic catholyte (1 M Li_2SO_4 + 1 M H_2SO_4) and (B) alkaline catholyte (2 M LiOH). Cell voltage responds immediately as oxygen/argon flow conditions are changed. Unmodified platinum mesh was used as the cathode current collector and carbon foam on stainless steel as the anode current collector. The anolyte solution is 2 M Li_2S_4 + 0.25 M LiOH in water. Discharge current density for both experiments is 0.065 mA/cm^2. Confirmation of Li- and Na-salt limited capacity in modified H cells using 4 M S anolyte with (C) 0.5 M Li_2SO_4 catholyte, and (D) 0.5M Na_2SO_4 catholyte. Each was cycled over the entire capacity range afforded by the salt concentration in the starting catholyte.

and anode. Cell tests were conducted in the temperature range 25°C–70°C, within which increasing the temperature was observed to dramatically reduce cell impedance. Increasing temperature also sharply increases Na_2SO_4 solubility in the catholyte beginning at about 35°C.[19,20]

Galvanostatic step charges and discharges produced voltage efficiency results shown in Figures 5A and 5B for Li and Na chemistry, respectively. Values plotted are the round-trip voltage efficiency, i.e., the discharge voltage divided by the charge voltage. Using the acidic catholyte and dual catalysts (IrO_2 for OER and Pt black for ORR), the voltage efficiency reaches 71%–74% for both Li and Na solutions at low current density (0.065 mA/cm^2). Here, efficiency is limited by the OER/ORR reaction. Using a less efficient, Pt mesh, single cathode rather than the dual cathodes with IrO_2/Pt black catalysts, and holding all other cell parameters constant, the voltage efficiency at 70°C is about 20% lower, as shown in the Supplemental Information (Figure S2).

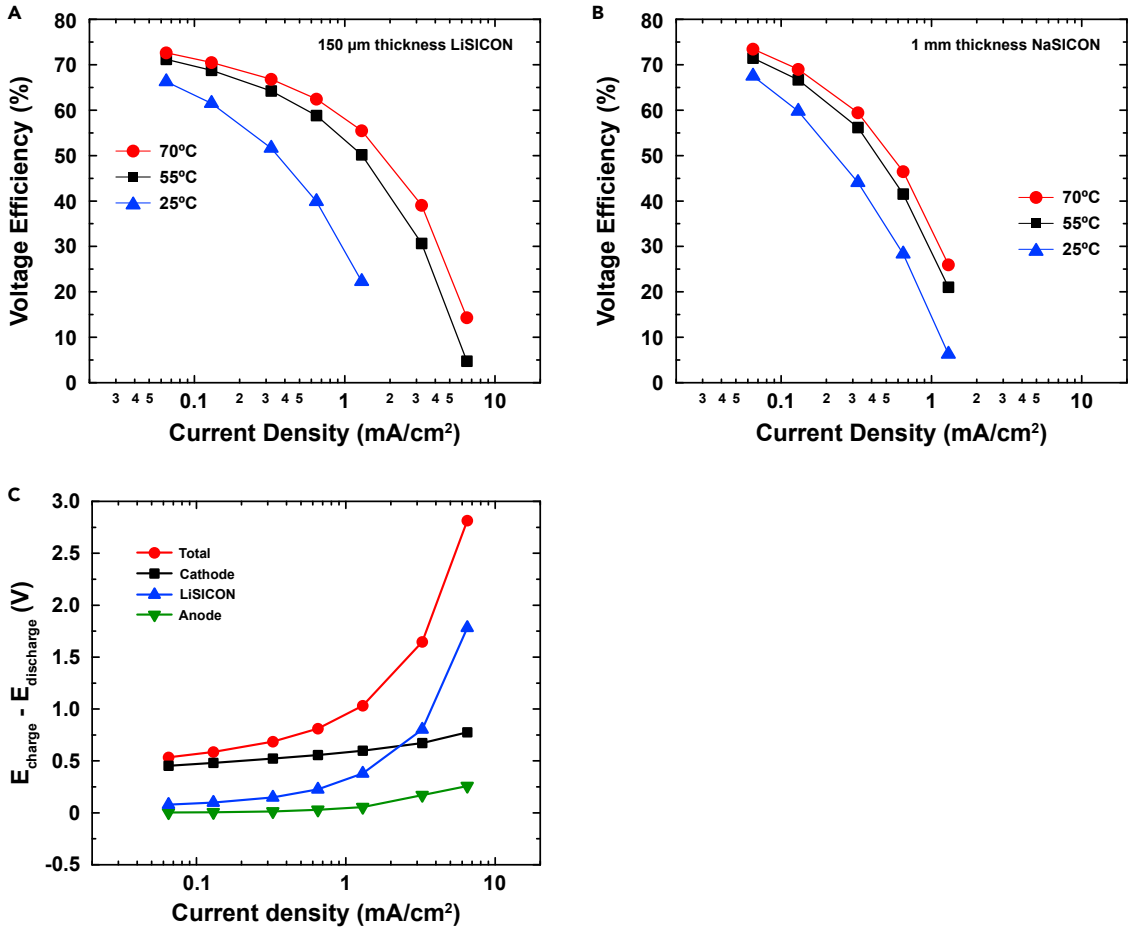

Figure 5. Voltage Efficiency as a Function of Current Density at 25°C, 55°C, and 70°C, for Acidic Catholyte and Alkaline Anolyte

(A) Li chemistry and 150-µm-thick LiSICON membrane.

(B) Na chemistry and 1,000-µm-thick NaSICON disk. At the lowest current densities, the round-trip efficiency is limited to 71%–74% by the OER and ORR reactions.

(C) With increasing current density, the ceramic membrane resistance becomes limiting. Sources of polarization determined by a cell using dual reference electrodes, an alkaline Hg/HgO (in 1 M LiOH) reference electrode at the anolyte side and an Hg/Hg_2SO_4 (in saturated K_2SO_4) reference electrode at the catholyte side at 55°C. Polarization due to membrane resistance dominates over that due to the catholyte and anolyte redox reactions at current densities higher than about 2 mA/cm^2. All cells used a stainless-steel mesh anode and dual cathodes with catalysts (IrO_2 for OER and Pt black for ORR). Gas flow at the catholyte side was oxygen gas during ORR and argon gas during OER. The anolyte was 1 M Li_2S_4 + 1 M LiOH and the catholyte was 0.5 M Li_2SO_4 + 0.1 M H_2SO_4.

With increasing current density, the voltage efficiency decreases since additional contributions to impedance become significant. The results in Figure 5A were obtained using a 150-µm-thick LiSICON membrane, with a measured ionic conductivity of 0.28 mS/cm at room temperature and 0.6 mS/cm at 55°C, whereas the results in Figure 5B were obtained using a NaSICON membrane of higher ionic conductivity, 2 mS/cm at room temperature,[21] but also much greater thickness of 1,000 µm. We conducted most of our experiments using Li chemistry simply due to the greater availability of LiSICON membranes. To separate the membrane resistance from other contributions, an experiment was conducted using two different reference electrodes, an alkaline Hg/HgO (in 1 M LiOH) reference electrode at the anolyte side and a Hg/Hg_2SO_4 (in saturated K_2SO_4) reference electrode at the catholyte side. A stainless-steel mesh anode current collector and dual cathodes with IrO_2 and Pt black catalysts were used. Step-galvanostatic scans consisting of sequential

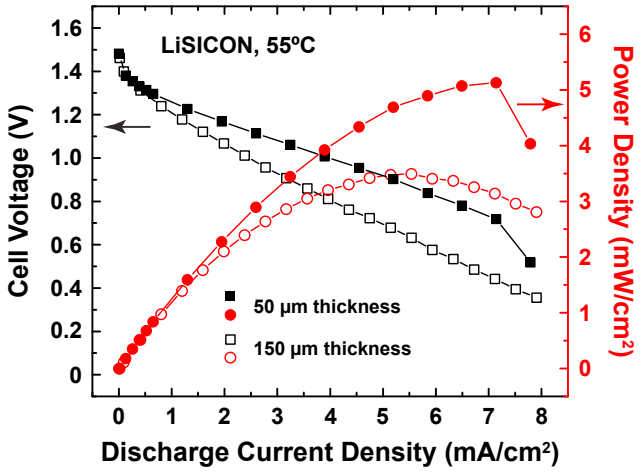

Figure 6. Polarization and Power Density versus Current Density for Li Chemistry, Measured at 55°C in H Cells Using Two Different Thicknesses of LiSICON Membrane

The cell with the 50-µm-thick membrane shows reduced polarization and a higher power density (peak value of 5.1 mW/cm^2 at 7.1 mA/cm^2), compared with the cell with the 150-µm-thick membrane of the same composition (peak power density of 3.4 mW/cm^2 at 5.5 mA/cm^2).

5 min galvanostatic charge or discharge at various current densities were performed while measuring voltage. The overall polarization is obtained from the voltage difference between cathode and anode, the cathode contribution from the voltage between cathode and Hg/Hg_2SO_4 reference electrode, and the anode contribution from the voltage between anode and Hg/HgO reference electrode. Figure 5C plots the total polarization and the cathode, anode, and membrane contributions as a function of current density, using the 150-µm-thick LiSICON membrane. It is seen that the cathode and anode polarization remain relatively constant, with the anode polarization being lower by at least a factor of five over the measured current density range (up to 7 mA/cm^2). The membrane polarization, on the other hand, increases with current density, and is about 50% of the total impedance at current density of 3 mA/cm^2.

Further evidence that polarization and power density in the current unoptimized design are primarily limited by membrane resistance appears in Figure 6, where the polarization and power density of H cells were measured for two LiSICON membranes with different thicknesses (both at 55°C using a single Pt mesh cathode coated with Pt black). With the thinner membrane of 50 µm thickness, decreased polarization is evident and a higher power density with peak value of 5.1 mW/cm^2 at 7.1 mA/cm^2 was reached. In comparison, a 150-µm-thick membrane of the same composition yielded a peak power density of 3.4 mW/cm^2 at 5.5 mA/cm^2. These values of power density are low compared with those for polymer-membrane-based redox flow batteries or proton exchange membrane (PEM) fuel cells, and may be significantly improved if membrane resistance is lowered. Nonetheless, we use these experimentally observed values as starting input parameters in the techno-economic (T-E) model for the flow battery, discussed later.

Another important cost factor is the cost of catalyst required to support a given power density. Several non-platinum group metal (PGM) catalysts for OER and ORR in acid media have been proposed,[22–25] which we are in the process of evaluating. However, we have also investigated the impact of Pt black loading on the charge-transfer resistance of the experimental flow cell (Figure 3D), using galvanostatic

electrochemical impedance spectroscopy (GEIS). The US Department of Energy's (DOE) future PEM fuel cell total PGM target for Pt loading is 0.15 mg/cm^2,[26] but this loading accommodates about 100 times higher power density (800 mW/cm^2) than is assumed in our model. Experiments were conducted using two Pt black loadings, one higher (0.21 mg/cm^2) than the DOE target and one a factor of five lower (0.03 mg/cm^2). We found that the impact of temperature was much greater than the impact of loading. Figure 7A shows selected Cole-Cole plots from these measurements, in which the higher frequency arc is due to membrane impedance and the lower frequency arc is correlated with ORR kinetics.[27] A small inductive loop at the lowest frequencies is observed in each case, consistent with the literature,[27] which we did not attempt to fit. Figure 7B summarizes the GEIS results as a plot of total cell area-specific resistance (ASR) versus temperature. It is seen that the curves converge with increasing temperature such that at 50°C and above, neither current density nor loading significantly changes the ASR. At lower temperature where results are more differentiated, increasing discharge current density (comparing the red and black curves in Figure 7A) primarily decreases the ORR charge-transfer resistance, consistent with Butler-Volmer behavior whereby a larger overpotential results in faster kinetics. Increasing temperature (comparing blue and black curves in Figure 7A) decreases both membrane and ORR impedance. Increasing the catalyst loading with other parameters held constant (comparing blue and green curves) decreases the ORR charge-transfer resistance, but only at the lower temperatures, and does not change the membrane resistance. We use these results later for T-E modeling of the flow battery. Unlike Pt black, IrO_2 is not readily available as high surface area powder, so the impact of its loading on OER kinetics during charging was not investigated. In the T-E modeling, we assume similar loadings as for Pt black.

Deep Cycling Tests of Catholyte and Anolyte Stability

The ability of the catholyte and anolyte to undergo sustained deep cycling, and the durability of the cell components in contact with catholyte and anolyte, were tested using modified H-cell designs (Figures 3B and 3C). To test the catholyte, cells were assembled in which the catholyte capacity was lower than the anolyte capacity (provided by a 4 M S solution). Using a single cathode (Pt mesh), galvanostatic cycling (0.325 mA/cm^2) was conducted at room temperature, with the capacity during each cycle being limited to 96% of the catholyte theoretical capacity, based on the starting alkali ion concentration. Results are shown in Figure 8A, plotted as voltage-capacity curves for the 1st, 10th, 20th, and 30th galvanostatic charge/discharge cycles, spanning a total test time of over 1,600 hr. Dry air was continuously flowed into the catholyte chamber via a dispersion tube during discharge, and water was periodically added to the catholyte to compensate for evaporation. Initially, we chose to use capacity-limited cycling out of concern that proton intercalation into the LiSICON might occur upon the exhaustion of Li^+ without a clear voltage indication. However, as seen in Figure 8A, and in expanded scale in Figure S3, the charge curves are almost invariant after the first charge, indicating that the results would be nearly identical if a voltage cutoff were used. The slope of the voltage profile clearly deviates toward the end of the charge (Figure S3) as expected from an increased mass transfer resistance resulting from the depletion of working ion (Li^+). The minor variations in polarization for the discharge curves were found to be correlated with fluctuations in catholyte water level and air flow rate, which are expected to affect ORR kinetics. Over the >2 month duration of the test, the cell impedance did not grow detectably, pointing to good stability of the LiSICON membrane in contact with the acidic catholyte as well as stability of catholyte and anolyte with their respective electrodes, Pt mesh and stainless steel. (The voltage efficiency in these tests is low

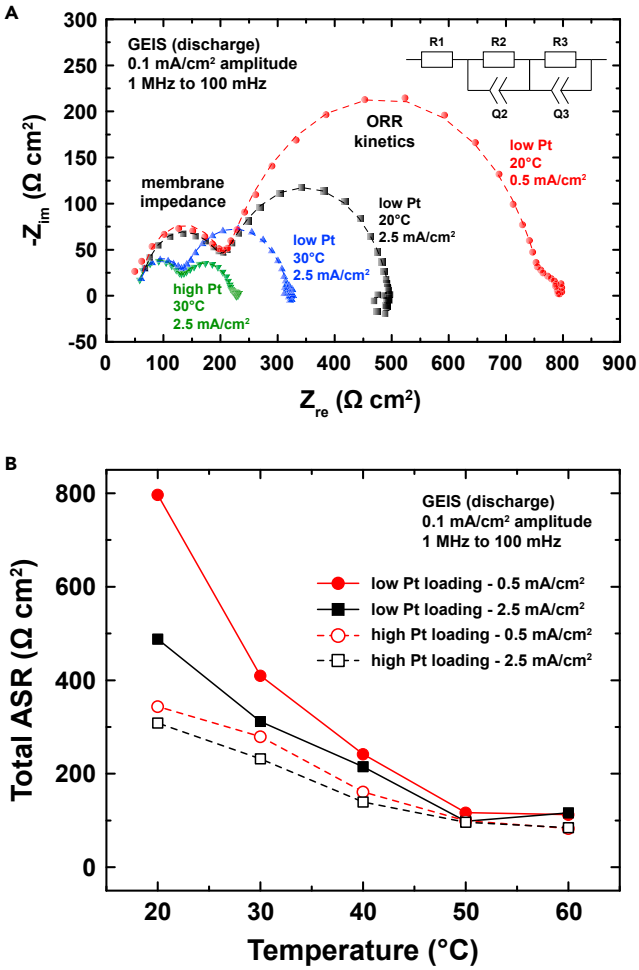

Figure 7. Galvanostatic Electrochemical Impedance Spectroscopy Study of the Air-Breathing Aqueous Sulfur Flow Cell during Discharge

Two Pt loadings were investigated: A high loading of 0.21 mg/cm^2 and low loading of 0.03 mg/cm^2, at two discharge current densities (0.5 mA/cm^2 and 2.5 mA/cm^2) and at five temperatures (20°C, 30°C, 40°C, 50°C, and 60°C.) A LiSICON membrane of 150 μm thickness was used, the catholyte contained 15 mL 0.5 M Li_2SO_4 + 0.5 M H_2SO_4 and anolyte contained 15 mL 0.5 M Li_2S_2 + 0.25 M Li_2S_4 + 1.25 M LiOH. The electrolyte flow rate was 0.5 mL/min and the air flow rate was 10 cm^3/min. Fixed amplitude (0.1 mA/cm^2) and frequency range (1 MHz to 100 mHz) were used throughout.

(A) Selected GEIS data plotted as area-specific impedance. In order of descending impedance, the data are for the following conditions. Red circles: low Pt loading, 20°C, 0.5 mA/cm^2. Black squares: low Pt loading, 20°C, 2.5 mA/cm^2. Blue triangles: low Pt loading, 30°C, 2.5 mA/cm^2. Green triangles: high Pt loading, 30°C, 2.5 mA/cm^2. The dotted lines are the corresponding fitted data for the two major semicircles based on the equivalent circuit shown in the inset.

(B) Total cell ASR versus temperature for low Pt loading (closed symbols) and high Pt loading (open symbols), and current densities of 0.5 (circle) and 2.5 (square) mA/cm^2. Each data point is the average of five measurements.

since they are conducted at room temperature and only use the single Pt mesh cathode for OER and ORR.)

In the Supplemental Information, Figure S4, we show that extreme variations in either water loss or water excess (dilution of the catholyte), or interruptions in gas flow, cause large deviations in coulombic efficiency, but also that the cells are

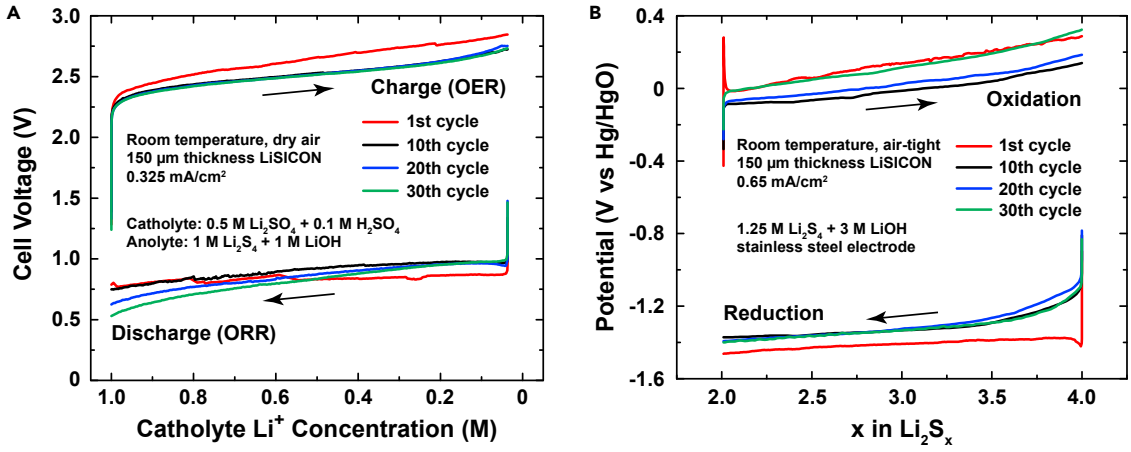

Figure 8. Long-Duration Cycling Tests of Catholyte and Anolyte

(A and B) Long-duration cycling tests of a typical (A) catholyte and (B) anolyte using modified non-flowing H cells shown in Figures 2B and 2C, respectively. (A) Air-purging cell cycles with 1 M Li^+ acidic catholyte over 96% of the total capacity against an excess of polysulfide anolyte. Stable cycling is observed during 30 cycles accumulated over 1,600 hr total test time at room temperature. Observed polarization is predominantly due to the resistance of the 150-μm-thick LiSICON membrane. (B) Symmetric cell test of 5 M S anolyte over Li_2S_2-Li_2S_4 composition range, using a 150-μm-thick LiSICON membrane. Active sulfur concentration was 1.25 M S (2.5 M electrons). The Hg/HgO (1 M NaOH, ~0.1 V versus standard hydrogen electrode) was placed in the counter electrode side, and thus the potential obtained on the working electrode (versus Hg/HgO as shown in the figure) refers to the electrode potential plus the iR_{cell} between the working electrode and the reference electrode. Stable cycling is observed over 30 cycles corresponding to 720 hr total test time at room temperature.

tolerant of such variations and return to stable operation once the water content and gas flow at the cathode are restored to their initial values.

Cycling stability of the polysulfide anolyte was tested in cells with two gas-tight chambers of differing volume containing the same anolyte, thus deeply cycling the smaller chamber (Figure 3C). LiSICON membrane and stainless-steel electrodes were used, and an alkaline Hg/HgO in 1 M LiOH reference electrode was placed in the larger chamber. Selection of the appropriate speciation range over which to cycle the anolyte requires consideration of complex equilibria.[28–30] Aqueous alkali-metal polysulfide solutions contain a wide range of species, including the alkali-metal cations (Li^+, Na^+, or K^+), H_2O, OH^-, H^+, H_2S, HS^-, S^{2-}, S_2^{2-}, S_3^{2-}, S_4^{2-}, and S_5^{2-}. Polysulfide solubility and stability are strongly dependent on pH,[12,29] alkali-metal cation,[30] nominal polysulfide speciation, and concentration[31] as well as temperature.[32] At low pH (<7), HS^- is the primary species, and the H_2S molecule is the predominant reduced product in the polysulfide solution.[29,33] At intermediate alkalinity (pH 9–14), the primary polysulfide species are S_4^{2-} and S_5^{2-} instead of HS^-,[29] although without good sealing H_2S may still be generated at pH ≈ 12, especially during the reduction reaction.[12] In a recently reported lithium polysulfide/$LiMn_2O_4$ battery, adding porous SBA-15 silica adsorbent to the polysulfide anolyte was found to reduce irreversible capacity loss and to improve capacity retention.[13] The improvements were attributed to the suppression of gaseous H_2S release, preventing continuous loss of sulfur. In highly alkaline polysulfide solution (e.g., >3 M OH^-), the predominant species are $S_3^{2-}$and S_2^{2-}.[34] A Li_2S_4 solution under these conditions may disproportionate into S^0 and S_2^{2-}/S_3^{2-} during long-term storage.[29,34] At temperatures above 80°C, thiosulfate is readily formed via the reaction S_n^{2-} + $m$$OH^-$ → $S_{n-m}O_m^{2-}$ + $m$$HS^-$.[32,35] This parasitic disproportionation reaction is detrimental to the stability of polysulfide anolyte, but slow at moderate temperature.[34,36]

Taking into account these prior studies, we prepared starting polysulfide solutions containing nominal stoichiometry Li_2S_4 and 1 M or 3 M LiOH at room temperature, and operated cells from room temperature up to 70°C, such that the starting predominant sulfur species is S_4^{2-} and the major degradation reactions are minimized. To date, we have found that the most stable cycling is obtained when we constrain the composition range to Li_2S_2 to Li_2S_4 or Na_2S_2 to Na_2S_4; see Figure 8B for cycling results at 5 M S concentration obtained over 720 hr. In the interest of increasing energy density and further lowering cost, the ability to reversibly cycle beyond the Li_2S or Na_2S solubility limit is desirable. Our group has previously shown that percolating nanocarbon suspensions can be used to improve charge transfer in fluid electrodes to the extent of realizing reversible precipitation of Li_2S.[37,38] A similar strategy could be applied here to extend the polysulfide capacity range.

Demonstrating an Air-Breathing Flow Cell

Having independently demonstrated each component of the system in a non-flowing cell, we then tested the air-breathing flow cell system with a continuously pumped supply of both catholyte and anolyte (Figure 9A). Design details of the cell are given in Experimental Procedures and shown in Figure 3D. In order to have a true air-breathing cell, an acidic Li_2SO_4-based catholyte was used; for an alkaline catholyte, it is expected that some form of CO_2 exclusion or trapping would be necessary to prevent trace carbon dioxide present in air from reacting with the base to precipitate lithium or sodium carbonate during long-term operation. For ease of handling and assembly, we used the 150-μm-thick LiSICON membrane, although it was recognized that its resistance would dominate the ASR of the cell at room temperature. Figure 9B shows the polarization and power density of the flow cell measured at 55°C with an air stream feeding the air chamber. On discharge, the flow cell delivers a peak power of 3.2 mW/cm^2 at 6.0 mA/cm^2, which is consistent with the result from the static counterpart in Figure 6 (3.4 mW/cm^2 at 5.5 mA/cm^2, under pure oxygen flow). Extended cycling of the flow cell system was then performed at room temperature. Figure 9C shows charge-discharge curves for cycling under air-breathing conditions at 0.325 mA/cm^2 for 40 cycles, spanning a total test time of 960 hr. The relatively stable charge/discharge curves reflect a stable membrane impedance, which was separately validated by impedance measurements of the cell after 720 hr, shown in Figure S5. We did observe sulfur precipitation (verified by energy-dispersive X-ray analysis of the precipitate) in the anolyte reservoir after about every 10 cycles (240 hr) and replaced the anolyte at those intervals. Since the sealed non-flowing cell (Figure 8B) did not exhibit detectable sulfur precipitation, whereas a deliberately air-exposed anolyte did (in a separate experiment), we attribute the precipitation in the flow cell to an air leak in the anolyte circuit. The round-trip voltage efficiency of the air-breathing flow cell at 55°C and a current density of 0.325 mA/cm^2 is ~55% (Figure 9C). Results in Figure 7 show that at this temperature, the ASR is no longer dependent on the Pt loading and is dominated by the membrane resistance. At room temperature, the voltage efficiency drops to ~43%, and operating the cell at a higher current density of 2 mA/cm^2 at 50°C resulted in a round-trip voltage efficiency of ~33% (Figure S6), again limited by membrane resistance as shown by Figure 5C. These tests demonstrate proof-of-concept operation of the proposed air-breathing aqueous sulfur flow battery. Clearly, decreased membrane resistance is necessary to reach higher round-trip efficiency and at higher current densities. Several possible paths to more highly conductive membranes for this application are currently under study.

Techno-economic Analysis and Comparison with Other Approaches

Flow batteries, by virtue of their design allowing independent scaling of power and energy, have a cost structure similar to that of PHS and CAES. The total cost of these technologies can be separated into costs for the power-generating reactor and the

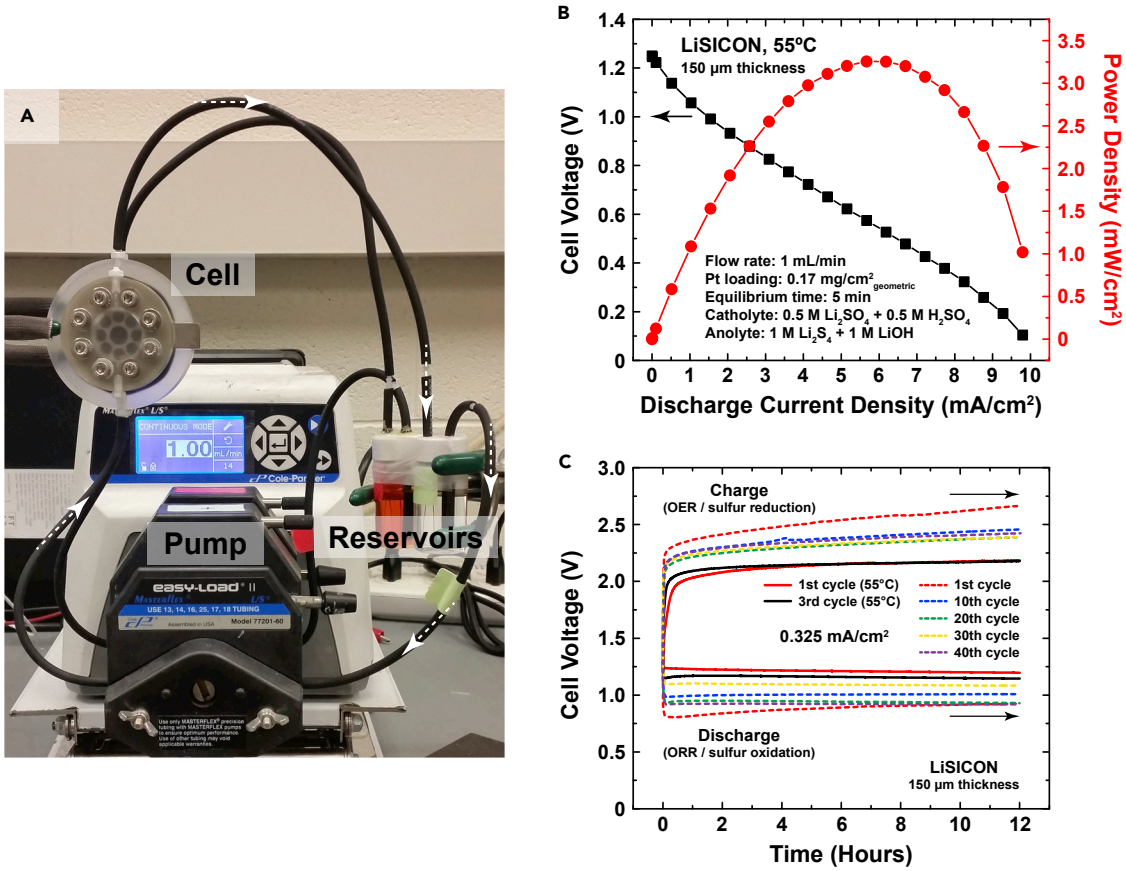

Figure 9. The Power and Cycling Performance of a Laboratory-Scale Air-Breathing Aqueous Sulfur Flow Cell

(A) Laboratory-scale flow battery combining an air-breathing cell with continuously flowing catholyte and anolyte.

(B) Polarization and power density versus current density, measured at 55°C under 1 mL/min fluid flow rate.

(C) Select cycles of voltage-time curves measured at room temperature and 0.325 mA/cm^2 for 40 cycles, corresponding to 960 hr of continuous operation. The 1st and 3rd cycles of voltage-time curves at 55°C at the same current density are shown as the dotted lines. The catholyte contained 10 mL of 0.5 M Li_2SO_4 + 0.5 M H_2SO_4 and the anolyte contained 10 mL of 1 M Li_2S_4 + 1 M LiOH. The electrolyte flow rate is fixed at 1 mL/min. During charge, no gas was supplied to the cell. During discharge, dry air was supplied at 10 cm^3/min to the air chamber for convective air breathing. The anolyte was replaced every 10 cycles (240 hr) due to sulfur precipitation, attributed to accidental air ingress in the anolyte circuit.

energy-storing reservoirs, plus certain additional costs. For PHS and CAES, the cost of power (e.g., US$/kW) is primarily determined by the cost of power-generating turbines and associated equipment, whereas for flow batteries, it is primarily the cost of the power-generating stack. The cost of energy (e.g., US$/kWh) is primarily determined by size of the storage reservoir in the case of PHS and CAES, and by the chemicals and tanks in the case of flow batteries. At system level, the cost of energy (US$/kWh) is the ratio of power cost (US$/kW) to total storage duration (hr), the former being defined by the cost of the storage reservoirs or tanks and the working fluids within. Thus, a useful way to display the cost of storage is as a log-log plot of installed cost (US$/kWh) versus E/P ratio (hr) (Figure 10). This plot allows the cost of storage technologies to be compared on an equal basis. In the limit of long storage duration (>1 month), the cost asymptotically approaches the cost of energy alone, as the cost of the power-generating stacks or turbines becomes negligible. As the storage duration shrinks, the power cost constitutes an increasing proportion of the total cost. Our T-E model is based on the flow battery model for future-state battery price developed by Darling et al.,[16] to which adjustments were made to arrive at an installed cost that can be directly compared with the installed costs of PHS and

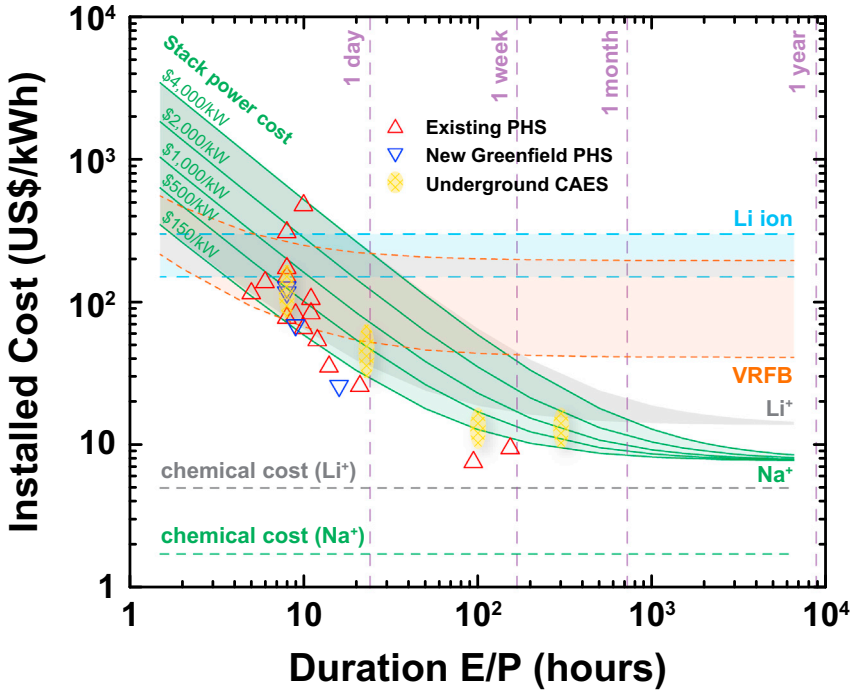

Figure 10. Installed Cost versus Storage Duration for Several Energy Storage Technologies

For a Figure360 author presentation of Figure 10, see the figure legend at https://doi.org/10.1016/j.joule.2017.08.007#mmc2.

Curves for the present air-breathing aqueous sulfur flow battery approach using Na and Li chemistry are shown in green and gray, respectively. The chemical costs for Na and Li are shown as dashed lines. Curves of constant power cost show that the power stack dominates the system cost at short storage durations, whereas at long duration the cost asymptotically approaches the energy cost due to chemical constituents plus storage tank and related costs. 5 M concentrations of both Na and S are assumed, with cycling of the sulfur over the speciation range S_2^{2-} to S_4^{2-} corresponding to 25% of theoretical capacity. The peak power density of the stack ranges from 4.3 mW/cm^2 at US$4,000/kW and US$2,000/kW to 28.6 mW/cm^2 at US$150/kW; details are given in the Supplemental Information. The projected costs for air-breathing aqueous sulfur compare favorably with those for pumped hydroelectric storage (PHS) and underground compressed air energy storage (CAES), while also having several-fold higher energy density and being free of the locational constraints faced by each.

CAES facilities. The methodology for calculating each of the cost contributions is explained in Experimental Procedures.

In arriving at the energy cost component of the cost curves in Figure 10, the anolyte sulfur concentration is assumed to be 5 M (the experimental flow cell in Figure 9 used 4 M), and the total catholyte concentration of Li^+ or Na^+ (added as Li_2SO_4 or Na_2SO_4) is 5.2 M, the excess salt relative to the nominal anolyte concentration (5 M) being added to avoid the onset of mass transfer limitations in the catholyte as it approaches the fully charged state. The resulting chemical costs for Li and Na chemistry are shown as horizontal dashed lines in Figure 10, and assume cycling only between S_2^{2-} to S_4^{2-}, corresponding to the experimentally demonstrated speciation range in Figures 8B and 9C. The Na chemical cost is US$1.7/kWh, and after accounting for tank cost (US$0.15/L) and other costs, the resulting energy cost for Na chemistry is a factor of 4–6 higher than the chemical cost alone. Thus, as with PHS and CAES, the energy-storing fluids have lower cost than the structures used to contain them.

The largest contributions to power cost come from the membrane and catalyst. Our current experiments use ceramic membranes, for which the US DOE has projected a cost, at high production volumes, of less than US$10/m^2.[39] In the cost model, we conservatively assume costs of US$10/m^2 and US$100/m^2. Alternative low-cost membranes such as polymer-ceramic composites[40] could also be developed for this application. The total PGM catalyst loading is assumed to be 0.05 mg/cm^2; the experimentally validated value in Figure 7 is 0.03 mg/cm^2 for the Pt black alone.

A remaining adjustable parameter in the power cost calculation is the ASR (R). Although we measured values of $R \sim 100\ \Omega \cdot m^2$ in the current laboratory flow cell, this is for an unoptimized lab cell, and improvements are to be expected. Thus, we use $R \sim 100\ \Omega \cdot m^2$ as the highest input value in the model. In Figure 10, cost curves are shown in which the power cost ranges from US$4,000/kW (4.3 mW/cm^2 peak power) to US$150/kW (28.6 mW/cm^2 peak power). The values for membrane cost, catalyst loading, and ASR corresponding to each curve are tabulated in Table S7. The highest power cost, US$4,000/kW, corresponds to a membrane cost of US$100/m^2 (more than ten times the DOE projection), and $R = 100\ \Omega \cdot m^2$. This power cost drops by half to US$2,000/kW if a membrane cost of US$10/m^2 is assumed. An additional factor of two reduction, to US$1,000/kW, is obtained assuming a relatively modest reduction in ASR, to $R = 55\ \Omega \cdot m^2$. Further reduction of power cost, to US$500/kW and US$150/kW, would be obtained if the ASR were reduced to $R = 30\ \Omega \cdot m^2$ and $15\ \Omega \cdot m^2$, respectively. Based on literature values for the resistivity of LiSICON and NaSICON[21,41], 150-μm-thick membranes should contribute bulk ASR at 55°C of only 24.5 and $1.5\ \Omega \cdot m^2$, respectively, and the ORR reaction according to literature[27] should contribute only $6\ \Omega \cdot m^2$. Our measurements (Figure 5C) show that membrane and ORR resistance are indeed the two largest contributions, so the assumed R values may well be achievable with further development. For example, the membrane resistance includes interfacial contributions that could be reduced by flow channel design.

To arrive at the installed cost, balance-of-plant costs and allowances for sales, administration, depreciation, warranty, R&D, and profit margin are included. Figure 10 compares the projected installed cost for the present approach with several other storage technologies suitable for large-scale stationary storage. The cost range of vanadium redox flow batteries (VRFB) is shown with lower and upper bound cost factors as calculated by Darling et al.[16] The cost of Li-ion batteries is also shown as a band that represents the range of 2030 projected costs for EV battery packs.[42] Given the relative inflexibility of the power to energy ratio in Li-ion battery design compared with flow batteries, we plot Li-ion costs as being independent of storage duration; this is a reasonable representation except at the shortest durations on this scale (<1 hr) where high-power and high-energy Li-ion batteries are differentiated. The PHS data are obtained from the Compendium of Pumped Storage Plants in the United States[43] for existing installations, and the DOE/EPRI Electricity Storage Handbook[44] for four new "greenfield" sites, as listed in Table S9. Note that the costs of existing PHS installations have been adjusted for inflation, an important correction without which the cost of PHS can be underestimated by up to a factor of >5 for the oldest US plants. Only United States PHS facilities and only those in which storage capacity is generated by pumping alone are included; we have excluded those benefiting from riverine flows, which may have artificially low costs of energy. The cost of CAES is taken from Appendix B of the DOE/EPRI Electricity Storage Handbook[44] and an analysis of long-duration storage (100–300 hr) storage for levelizing the output of wind farms.[45]

In Figure 10 one sees, firstly, that the projected cost of air-breathing aqueous sulfur flow batteries has a similar dependence on storage duration to PHS and CAES. This shared characteristic is due to the low baseline energy cost of all three approaches. The installed cost is dominated by the power stack cost at short discharge times and declines with increasing storage duration to asymptotically approach, at long discharge times, the energy cost alone. Beyond cost-competitiveness with PHS and CAES, the proposed battery has numerous other advantages, chief among which are higher energy density and locational flexibility. For the solution concentrations assumed in Figure 10, the chemical energy density (catholyte + anolyte) is 60 Wh/L; at system scale the energy density may be 20–40 Wh/L. This is a factor of 500–1,000 higher than the energy density of a typical PHS facility. Such electrochemical storage is also free of the highly restrictive geographical and environmental constraints that have limited growth of PHS and CAES. The batteries could be deployed as large systems of many MWh, or as smaller systems in a highly distributed manner, allowing a broader range of use models (e.g., residential storage) than is possible with PHS or CAES. To illustrate the likely size of distributed storage units, we have modeled in the Supplemental Information (see Figure S7) the installed cost of a 12 kW system. With increasing energy, the system cost declines, reaching US$100/kWh at 125 kWh of storage, corresponding to a 10.5 hr discharge time. The volume of such a system is 4.6 m^3, of which 2.1 m^3 is the electrolyte volume (calculated for an energy density of 60Wh/L).

Electrochemical storage approaches with ultralow energy cost, which best express their advantages in systems designed for long storage durations, may become increasingly attractive as the percentage of renewable generation on the electric grid increases. Figure 10 shows that below about 10 hr duration, multiple technologies can compete on a cost-of-energy basis; these may be differentiated on the basis of other factors not shown here, such as energy density and round-trip efficiency at high charge/discharge rates. Beyond 10 hr duration, where heretofore PHS and CAES have had the cost advantage, the air-breathing aqueous sulfur flow battery offers a new low-cost option. Consider the long-duration CAES case study included in Figure 10, in which 100–300 hr storage was found to be necessary to fully smooth the output of a single wind farm and produce baseload power.[45] At <US$2,000/kW power cost, the present approach matches the cost, while not requiring underground caverns for storage. Renewable generation may not be "stranded," however, and intermittent generation can be smoothed by aggregating multiple wind or solar farms, and by mixing renewable resources, at the expense of interconnection infrastructure.[46] Nonetheless, a detailed cost-minimization model combining wind, solar, and electrochemical storage resources for a large regional grid (the PJM Interconnection, 31.5 GW) has shown that as the cost of storage is reduced, lower electricity cost is obtained by integrating storage over longer duration.[47] For example, the storage duration at which electricity cost is minimized increases from 9 hr for Li-ion batteries (lithium titanate chemistry) to 72 hr for a fuel cell/electrolyzer system with gaseous hydrogen storage in pressure-rated steel tanks (at a cost of 41–102 US$/kWh for the tanks alone).[48] Thus, the long storage duration regime is expected to become increasingly important as electricity production by solar and wind grows in proportion to fossil-fuel-based generation.

In summary, this work demonstrates a new electrochemical storage approach that uses an aqueous polysulfide anolyte in conjunction with an air-breathing catholyte to reach exceptionally low chemical cost of storage (~US$1/kWh) while providing moderately high energy density (29–121 Wh/L at the solution level). The chemical cost of stored energy is one of, if not the, lowest among known rechargeable

batteries. Implemented in a flow battery architecture, this approach could offer the cost/performance characteristics of PHS and CAES, today the lowest-cost and most widely scaled energy storage technologies, while being free of geographical and environmental constraints and having up to a 1,000 times higher energy density at system level. Techno-economic modeling shows that at the current stage of development, stack power cost is the limiting cost factor. A modest reduction in stack resistance over current laboratory results would allow power cost of US$1,000–2,000/kW to be reached, competitive with PHS and CAES. This is achievable while using ceramic membranes and PGM catalysts as in the current experiments. Nonetheless, the scalability and cost of the flow battery could be significantly improved through development of low-cost low-resistance membranes, such as ceramic/polymer composite membranes,[40] and non-PGM OER[24,25] and ORR[22,23] catalysts. With further development, a new ultralow-cost electrochemical storage option may become available to support the growth of intermittent renewable generation and decarbonization of the world's energy systems.

EXPERIMENTAL PROCEDURES

Materials

Sulfur (S, ≥99.5%), lithium sulfate monohydrate ($Li_2SO_4 \cdot H_2O$, ≥99.0%), and sodium sulfate (Na_2SO_4, ≥99.0%) were purchased from Sigma-Aldrich. Lithium sulfide (Li_2S, 99.9%), sodium sulfide nonahydrate ($Na_2S \cdot 9H_2O$, 98.0% min.), Pt black, Pt wire or mesh (Pt, ≥99.9%), nickel (Ni) and stainless-steel mesh, and iridium oxide powder (IrO_2, 99%) were purchased from Alfa Aesar. For ion-selective membranes, we used a lithium superionic conductor (LiSICON, LIGCG Plate [AG-01]; Ohara Corp., Sagamihara-Shi, Kanagawa, Japan) and a sodium superionic conductor (NaSICON membrane; Ceramatec, Salt Lake City, Utah, USA) for the Li^+- and Na^+-based chemistries, respectively. Several types of reference electrodes were used in the three-electrode electrochemical cells. An Ag/AgCl reference electrode filled with 3 M NaCl solution (Bioanalytical Systems, Inc.) or Hg/Hg_2SO_4 reference electrode filled with saturated K_2SO_4 solution (CH Instruments, Inc.) were used at the acidic catholyte side. An Hg/HgO reference electrode filled with 1 M LiOH or 1 M NaOH solution (CH Instruments, Inc.) was used in the alkaline polysulfide solution. Carbon foam (Duocell reticulated vitreous carbon foam, 3% normal density; ERG Aerospace Corp.) was used in some experiments as the polysulfide current collector. The flow cell used a gas diffusion layer (SGL 35BC; Ion Power, DE, USA).

Catholyte and Anolyte Solutions

Cell tests were performed using acidic and alkaline catholytes, Li^+ and Na^+ working ions, and oxygen- and air-breathing cell configurations. The catholyte was prepared by dissolving Li_2SO_4 or Na_2SO_4 in 0.1 M or 0.5 M H_2SO_4 (Mallinckrodt, Inc.; 95.7%) solution. The molar concentrations of Li_2SO_4 or Na_2SO_4 in the catholyte are specified for each experiment.

In most of our tests, anolyte concentrations of 4 mol S/L (equivalent to 8 mol electrons/L) were used, although some experiments were conducted with 5 M S. These concentrations are still less than half of the sulfur solubility limit at room temperature. Note that typical aqueous flow batteries use active species concentrations of 1–2 M, and unlike sulfur, most of these species cannot support multi-electron transfer.[49]

The anolyte solutions contained Li_2S_4 or Na_2S_4 as the starting polysulfide composition, and were prepared using the following steps. S, Li_2S, or Na_2S, and LiOH or NaOH were mixed in a targeted molar ratio and added to deionized water. LiOH or NaOH was used to adjust the solution pH. The mixture was vigorously stirred in

an air-tight bottle until a transparent yellowish solution was formed. Since alkali-metal polysulfide solutions contain a wide range of sulfide species, an Li_2S_4 (or Na_2S_4) anolyte composition refers to a nominal S/Li_2S ratio of 3:1.

Non-flowing Electrochemical Cell Designs

Three types of non-flowing electrochemical cells were used, shown in Figures 3A–3C. Standard H cells with a cell membrane area of ~1.5 cm^2 and electrolyte volume of ~5 mL (Figure 3A) were used in shallow-cycling tests to validate the half-cell reactions and to characterize voltage efficiency. In these cells, the low membrane area to electrolyte volume, 0.3 cm^{-1}, restricts the total current through the membrane to values that imply very long cycle times (low C rates).

Two modified H cells were therefore designed to allow deep cycling tests of the catholyte (Figure 3B) and the anolyte (Figure 3C), respectively. The membrane to electrolyte ratio is 10-fold higher than the standard H cell at 3 cm^{-1}. Customized cell parts were fabricated by Adams & Chittenden Scientific Glass and modified as needed. The LiSICON or NaSICON membrane was sandwiched between two silicone rubber O rings that are attached to the glass chambers. The assembly was clamped to ensure good sealing; the anolyte chamber feedthroughs are also sealed with epoxy resin to ensure an air-tight seal.

To catalyze OER/ORR at the catholyte side, we used either platinum mesh as a single cathode with bifunctional catalystic activity, or dual cathodes (Ti or Pt mesh) coated with IrO_2 as the OER catalyst and Pt black as the ORR catalyst. At the anolyte side, reticulated stainless steel, carbon foam on stainless steel, or sulfide-treated Ni mesh was used. A pH-separating membrane is required for cells that use acidic catholyte with alkaline anolyte; we used LiSICON and NaSICON for Li- and Na-based chemistry, respectively. For the case where the catholyte and anolyte are both alkaline, a polymeric membrane can in principle be used, although here we used LiSICON or NaSICON as well.

Air-Breathing Flow Cell Design

An air-breathing cell with simultaneously flowing catholyte and anolyte was used to demonstrate flow battery operation (Figure 3D). We did not attempt to optimize the power stack components for cost but used components with well-known electrochemical and physicochemical properties. A gas diffusion layer modified with Pt/C (50 wt % Pt on Vulcan), applied at the desired loading on a carbon microporous layer, was used as the ORR cathode. A separate platinized Ti screen coated with IrO_2 (~0.1 $mg/cm^2_{geometric}$) was used as the OER cathode. This dual-cathode configuration was used to avoid corrosion of the carbon during OER.[50] Sulfided Ni mesh, which was prepared by soaking Ni mesh in 1 M Li_2S_4 + 1 M LiOH solution at ~100°C for 1 hr, served as the catalytic anode for the anolyte half-reaction. A peristaltic pump (Masterflex, Cole-Parmer) circulated catholyte and anolyte through the electrode chambers at 1 mL/min. Dry air (Airgas, zero grade, total hydrocarbons <1 ppm) was supplied during discharge at a flow rate of 10 mL/min, controlled with a gas flow meter (Cole-Parmer). Grade 2 titanium (McMaster-Carr) and stainless-steel 316 (McMaster-Carr) plates were used as the current collectors at the cathodes and anode, respectively.

Electrochemical Measurements

All electrochemical tests were performed using Biologic VMP3 potentiostats. The test conditions are specified for each experiment. Electrochemical tests carried out at room temperature were subject to temperature variation between 23°C and

25°C. A thermostated, stirred water bath controlled to ±2°C was used to perform electrochemical tests at elevated temperature for the non-flowing cells and the polarization study of the flow cell. The non-flowing cells were directly immersed in the water bath. For the flow cell tests, the cell reservoirs and flow cell power stack were enclosed in a polyethylene bag and immersed in the water bath. A second thermocouple was used to monitor the temperature at the cell stack. The air-breathing flow cell cycling test at 55°C was performed in an environmental chamber (ESPEC) with a temperature variation of ±0.2°C.

Techno-economic Modeling of the Flow Battery

The energy cost (c_{energy}, US$/kWh) was calculated as follows:

$$c_{energy} = \frac{c_{chemical} + c_{tank}}{\varepsilon_{sys,d}\varepsilon_{q,rt}\varepsilon_{V,d}}, \quad \text{(Equation 1)}$$

where $c_{chemical}$ is the total chemical cost (US$/kWh); c_{tank} is the tank cost (US$/kWh); $\varepsilon_{sys,d}$ is the system efficiency during discharge, accounting for power conversion, pumping, heating, and/or cooling; $\varepsilon_{q,rt}$ is the round-trip coulombic efficiency; $\varepsilon_{V,d}$ is the discharge voltage efficiency (discharge voltage divided by cell open circuit voltage). $c_{chemical}$ combines the costs of all chemicals (US$/L) normalized by the energy density (kWh/L) as shown in Table S4. Cell assembly is assumed to occur in the discharged state using the chemicals and the corresponding concentrations listed in Table S5. The water cost (while minimal) is taken into account assuming 10% of the total volume of the electrolytes is occupied by the solutes. The assumed bulk prices for Na_2SO_4, Li_2SO_4, H_2SO_4, NaOH, LiOH, Na_2S, Li_2S, and S are listed in Table S3 c_{tank} is the bulk tank price (US$0.15/L,[16] normalized by the theoretical energy density (kWh/L) as shown in Table S5. In the denominator of Equation 1, $\varepsilon_{sys,d}$ is taken as a constant of 0.94; $\varepsilon_{q,rt}$ is taken as unity by assuming that there is no species crossover or side reactions (as was the case for our experiments using the LiSICON membranes). $\varepsilon_{V,d}$ is taken as a constant of 70%.

The power cost (c_{power}, US$/kW) of the flow battery is calculated as:

$$c_{power} = \frac{c_a R}{\varepsilon_{sys,d} U^2 \varepsilon_{V,d}(1 - \varepsilon_{V,d})}, \quad \text{(Equation 2)}$$

where c_a is combined stack component cost per unit area (US$/m^2); R is the total ASR of the cell ($\Omega \cdot m^2$); U is the open circuit voltage of the cell (V); and other terms are as defined earlier. c_a depends on the amount of each stack component and its unit cost, which are tabulated along with the sources in Table S6. In the denominator of Equation 2, $\varepsilon_{sys,d}$ is taken as a constant of 0.94;[16] U is 1.5 V as observed experimentally for an acidic catholyte cell. $\varepsilon_{V,d}$ is taken as the same voltage efficiency of 70% as in the energy cost calculation.

The installed cost (e.g., US$/kWh) is calculated as follows:

$$c_{installed} = \left(\frac{c_{power} + c_{bop}}{t_d} + c_{energy}\right) \times (1 + f_{install}) + \frac{c_{add}}{t_d}. \quad \text{(Equation 3)}$$

Included are the energy cost (c_{energy}, US$/kWh), the power cost ($c_{power}$, US$/kW), the balance-of-plant cost (c_{bop}, US$/kW), the storage duration (t_d, hours), system installation cost adjustment factor ($f_{install}$, installation cost/equipment cost), and "additional cost" (c_{add}, US$/kW). The c_{bop} term includes the costs of accessories, including heating/cooling equipment, state-of-charge and power managing electronics, and pumps, needed to run a flow battery system. The c_{add} term captures other costs such as sales, administration, depreciation, warranty, research and

development, profit margin, etc. for the installation of this energy storage system. For c_{bop} and c_{add}, we use 202.5 US$/kW and 87.5 US$/kW, respectively[16] as the corresponding averaged upper and lower bound values (at 95% confidence) for other aqueous redox flow batteries. The cost of system installation is assumed to be 20.5% based on averaging the installation cost adjustment factor ($f_{install}$) of six existing VRFB systems according to Appendix B of the DOE/EPRI Electricity Storage Handbook.[44] Note that this is at the high end of the tabulated range for flow batteries (4%–20.5%).

SUPPLEMENTAL INFORMATION

Supplemental Information includes Supplemental Experimental Procedures, 7 figures, and 10 tables and can be found with this article online at https://doi.org/10.1016/j.joule.2017.08.007.

AUTHOR CONTRIBUTIONS

Conceptualization, Z.L. and Y.-M.C.; Methodology, Z.L., M.S.P., L.S., K.X., and Y.-M.C.; Investigation, Z.L., M.S.P., L.S., K.X., P.-C.T., J.M.V., A.F.B. ,and S.L.E.; Writing – Original Draft, Y.-M.C., Z.L., and L.S.; Writing – Review and Editing, Y.-M.C., F.R.B,. Z.L., and L.S.; Supervision, Z.L., L.S., and Y.-M.C.; Funding Acquisition, Y.-M.C. and F.R.B.

ACKNOWLEDGMENTS

This work was supported as part of the Joint Center for Energy Storage Research, an Energy Innovation Hub funded by the U.S. Department of Energy, Office of Science, Basic Energy Sciences. We thank the following colleagues for helpful discussions: Dr. Longjun Li and Dr. Brett Helms at Lawrence Berkeley National Laboratory; Parvin Adeli and Prof. Linda Nazar at University of Waterloo; Dr. Kevin G. Gallagher at Argonne National Laboratory; Dr. Robert M. Darling at United Technologies Research Center; and Prof. Chi-Jen Yang at Duke University. We also gratefully acknowledge Ceramatec Inc., Salt Lake City, Utah, for providing the NaSICON membranes used in this work.

Received: May 16, 2017
Revised: July 7, 2017
Accepted: August 8, 2017
Published: October 11, 2017

REFERENCES

1. US Department of Energy (2015). Revolution now: the future arrives for five clean energy technologies–2015 update. https://energy.gov/eere/downloads/revolution-now-future-arrives-five-clean-energy-technologies-2015-update.

2. Mason, B. (1958). Principles of Geochemistry (John Wiley).

3. Wadia, C., Albertus, P., and Srinivasan, V. (2011). Resource constraints on the battery energy storage potential for grid and transportation applications. J. Power Sourc. *196*, 1593–1598.

4. Bruce, P.G., Freunberger, S.A., Hardwick, L.J., and Tarascon, J.-M. (2011). Li-O2 and Li-S batteries with high energy storage. Nat. Mater. *11*, 19–29.

5. Pang, Q., Liang, X., Kwok, C.Y., and Nazar, L.F. (2016). Advances in lithium–sulfur batteries based on multifunctional cathodes and electrolytes. Nat. Energy *1*, 16132.

6. Yang, Y., Zheng, G., and Cui, Y. (2013). Nanostructured sulfur cathodes. Chem. Soc. Rev. *42*, 3018–3032.

7. Hueso, K.B., Armand, M., and Rojo, T. (2013). High temperature sodium batteries: status, challenges and future trends. Energy Environ. Sci. *6*, 734–749.

8. Ge, S.H., Yi, B.L., and Zhang, H.M. (2004). Study of a high power density sodium polysulfide/bromine energy storage cell. J. Appl. Electrochem. *34*, 181–185.

9. Xia, Y., Yufit, V., and Brandon, N.P. (2015). Polysulphide air redox flow battery - a novel solution for grid scale energy storage. ECS meeting Abstracts MA2015-03, 654.

10. Zito, R. (1997). Process for energy storage and/or power delivery with means for restoring electrolyte balance. US Patent 5612148 A, filed April 13, 1994, and published March 18, 1997.

11. Visco, S.J., Nimon, Y.S., Katz, B.D., Jonghe, L.C.D., Goncharenko, N., Loginova, V., and Company, P.B. (2012). Aqueous electrolyte lithium sulfur batteries. US Patent 20130122334 A1, filed May 18, 2012, and published May 16, 2013.

12. Demir-Cakan, R., Morcrette, M., Leriche, J.-B., and Tarascon, J.-M. (2014). An aqueous electrolyte rechargeable Li-ion/polysulfide battery. J. Mater. Chem. A *2*, 9025–9029.

13. Demir-Cakan, R., Morcrette, M., and Tarascon, J.-M. (2015). Use of ion-selective polymer membranes for an aqueous electrolyte rechargeable Li-ion–polysulphide battery. J. Mater. Chem. A *3*, 2869–2875.

14. Li, L., and Manthiram, A. (2016). Long-life, high-voltage acidic Zn–Air batteries. Adv. Energy Mater. *6*, 1502054–1502060.

15. Brandon, N., Kucernak, A., and Yufit, V. (2012). Regenerative fuel cells. Patent WO 2012/038379 Al, filed September 19, 2011, and published March 29, 2012.

16. Darling, R.M., Gallagher, K.G., Kowalski, J.A., Ha, S., and Brushett, F.R. (2014). Pathways to low-cost electrochemical energy storage: a comparison of aqueous and nonaqueous flow batteries. Energy Environ. Sci. *7*, 3459–3477.

17. Ha, S., and Gallagher, K.G. (2015). Estimating the system price of redox flow batteries for grid storage. J. Power Sourc. *296*, 122–132.

18. Braff, W.A., Mueller, J.M., and Trancik, J.E. (2016). Value of storage technologies for wind and solar energy. Nat. Clim. Change *6*, 964–969.

19. Bharmoria, P., Gehlot, P.S., Gupta, H., and Kumar, A. (2014). Temperature-dependent solubility transition of Na2SO4 in water and the effect of NaCl therein: solution structures and salt water dynamics. J. Phys. Chem. B *118*, 12734–12742.

20. Zhu, W.-Y., Gu, Y., Zhang, L., Jing, H., Liu, B., Zhang, F.-B., Zhang, G.-L., and Xia, Q. (2015). Solubility of Na2CO3 and NaHCO3 in aqueous sodium sulfate solutions and its application to separating Na2CO3 and Na2SO4 salt mixtures. Ind. Eng. Chem. Res. *54*, 5345–5348.

21. Hayashi, A., Noi, K., Sakuda, A., and Tatsumisago, M. (2012). Superionic glass-ceramic electrolytes for room-temperature rechargeable sodium batteries. Nat. Commun. *3*, 856.

22. Lefèvre, M., Proietti, E., Jaouen, F., and Dodelet, J.-P. (2009). Iron-based catalysts with improved oxygen reduction activity in polymer electrolyte fuel cells. Science *324*, 71–74.

23. Wu, G., More, K.L., Johnston, C.M., and Zelenay, P. (2011). High-performance electrocatalysts for oxygen reduction derived from polyaniline, iron, and cobalt. Science *332*, 443–447.

24. Huynh, M., Bediako, D.K., and Nocera, D.G. (2014). A functionally stable manganese oxide oxygen evolution catalyst in acid. J. Am. Chem. Soc. *136*, 6002–6010.

25. Frydendal, R., Paoli, E.A., Chorkendorff, I., Rossmeisl, J., and Stephens, I.E.L. (2015). Toward an active and stable catalyst for oxygen evolution in acidic media: Ti-Stabilized MnO2. Adv. Energy Mater. *5*, 1500991.

26. Spendelow, J., and Marcinkoski, J. (2014). Fuel Cell System Cost (US Department of Energy).

27. Antoine, O., Bultel, Y., and Durand, R. (2001). Oxygen reduction reaction kinetics and mechanism on platinum nanoparticles inside Nafion®. J. Electroanal. Chem. *499*, 85–94.

28. Giggenbach, W. (1971). Optical spectra of highly alkaline sulfide solutions and the second dissociation constant of hydrogen sulfide. Inorg. Chem. *10*, 1333–1338.

29. Giggenbach, W. (1972). Optical spectra and equilibrium distribution of polysulfide ions in aqueous solution at 20.deg. Inorg. Chem. *11*, 1201–1207.

30. Licht, S. (1988). Aqueous solubilities, solubility products and standard oxidation-reduction potentials of the metal sulfides. J. Electrochem. Soc. *135*, 2971–2975.

31. Licht, S. (1987). An energetic medium for electrochemical storage utilizing the high aqueous solubility of potassium polysulfide. J. Electrochem. Soc. *134*, 2137–2141.

32. Giggenbach, W.F. (1974a). Equilibriums involving polysulfide ions in aqueous sulfide solutions up to 240.deg. Inorg. Chem. *13*, 1724–1730.

33. O'Brien, D.J., and Birkner, F.B. (1977). Kinetics of oxygenation of reduced sulfur species in aqueous solution. Environ. Sci. Technol. *11*, 1114–1120.

34. Peramunage, D., and Licht, S. (1993). A solid sulfur cathode for aqueous batteries. Science *261*, 1029–1032.

35. Giggenbach, W.F. (1974b). Kinetics of the polysulfide-thiosulfate disproportionation up to 240.deg. Inorg. Chem. *13*, 1730–1733.

36. Licht, S., Manassen, J., and Hodes, G. (1986). The high aqueous solubility of K 2 S and its effect on bulk and photoelectrochemical characteristics of Cd (SeTe)/S x = cells I. Polysulfide variation at constant sulfur/sulfide ratio. J. Electrochem. Soc. *133*, 272–277.

37. Chen, X., Hopkins, B.J., Helal, A., Fan, F.Y., Smith, K.C., Li, Z., Slocum, A.H., McKinley, G.H., Carter, W.C., and Chiang, Y.-M. (2016). A low-dissipation, pumpless, gravity-induced flow battery. Energy Environ. Sci. *9*, 1760–1770.

38. Fan, F.Y., Woodford, W.H., Li, Z., Baram, N., Smith, K.C., Helal, A., McKinley, G.H., Carter, W.C., and Chiang, Y.-M. (2014). Polysulfide flow batteries enabled by percolating nanoscale conductor networks. Nano Lett. *14*, 2210–2218.

39. U.S. Department of Energy (2016). ARPA-E funding opportunity Announcement IONICS DE-FOA-0001478. https://arpa-e-foa.energy.gov/.

40. Aetukuri, N.B., Kitajima, S., Jung, E., Thompson, L.E., Virwani, K., Reich, M.-L., Kunze, M., Schneider, M., Schmidbauer, W., Wilcke, W.W., et al. (2015). Flexible ion-conducting composite membranes for lithium batteries. Adv. Energy Mater. *5*, 1500265.

41. Ohara Corp. (2016). Lithium-Ion Conducting Glass-Ceramics. http://www.oharacorp.com/lic-gc.html.

42. Nykvist, B., and Nilsson, M. (2015). Rapidly falling costs of battery packs for electric vehicles. Nat. Clim. Change *5*, 329–332.

43. Task Committee on Pumped Storage of the Hydropower Committee of the Energy Division of ASCE. (1993). Compendium of Pumped Storage Plants in the United States (American Society of Civil Engineers).

44. Akhil, A.A., Huff, G., Currier, A.B., Kaun, B.C., and Rastler, D.M. (2015). DOE/EPRI 2013 Electricity Storage Handbook in Collaboration with NRECA (Sandia National Laboratory).

45. Ingersoll, E. (2011). Long Duration Storage for Baseload Wind (General Compression, Inc.).

46. Hand, M.M., Baldwin, S., DeMeo, E., and Reilly, J.M. (2012). Renewable Electricity Futures Study (National Renewable Energy Laboratory).

47. Budischak, C., Sewell, D., Thomson, H., Mach, L., Veron, D.E., and Kempton, W. (2013). Cost-minimized combinations of wind power, solar power and electrochemical storage, powering the grid up to 99.9% of the time. J. Power Sourc. *225*, 60–74.

48. Steward, D.M. (2009). Scenario Development and Analysis of Hydrogen as a Large-Scale Energy Storage Medium (National Renewable Energy Laboratory).

49. Weber, A.Z., Mench, M.M., Meyers, J.P., Ross, P.N., Gostick, J.T., and Liu, Q. (2011). Redox flow batteries: a review. J. Appl. Electrochem. *41*, 1137.

50. Li, L., Liu, C., He, G., Fan, D., and Manthiram, A. (2015). Hierarchical pore-in-pore and wire-in-wire catalysts for rechargeable Zn– and Li–air batteries with ultra-long cycle life and high cell efficiency. Energy Environ. Sci. *8*, 3274–3282.